Manuscript submitted Dec. 14, 1981; revised manuscript received March 3, 1982.

Any discussion of this paper will appear in a Discussion Section to be published in the December 1983 JOURNAL. All discussions for the December 1983 Discussion Section should be submitted by Aug. 1, 1983.

Publication costs of this article were assisted by Siemens Research Laboratory.

REFERENCES

1. S. P. Murarka, *J. Vac. Sci. Technol.*, **17**, 775 (1980).
2. S. P. Murarka, D. B. Fraser, A. K. Sinha, and H. J. Levinstein, *IEEE Trans. Electron Devices*, **ed-27**, 1409 (1980).
3. B. L. Crowder and S. Zirinsky, *IEEE J. Solid-State Circuits*, **sc-14**, 291 (1979).
4. T. Mochizuki, K. Shibata, T. Inoue, and K. Ohuchi, *Jpn. J. Appl. Phys.*, **17-1**, 37 (1978).
5. P. Campelletti *et al.*, "Proceedings of the 4th Int. Symposium on Silicon Materials, Science, and Technology," p. 608, Minneapolis, Minnesota, May 1981.
6. W. Beinvogl and B. Hasler, "Proceedings of the 4th Int. Symposium on Silicon Materials, Science, and Technology, p. 648, Minneapolis, Minnesota, May 1981.
7. D. Pawlik, Unpublished results.

Solidification-Front Modulation to Entrain Subboundaries in Zone-Melting Recrystallization of Si on SiO_2

M. W. Geis, Henry I. Smith,[1] D. J. Silversmith,* and R. W. Mountain

Lincoln Laboratory, Massachusetts Institute of Technology, Lexington, Massachusetts 02173

and C. V. Thompson

Research Laboratory of Electronics, Massachusetts Institute of Technology, Cambridge, Massachusetts 02139

ABSTRACT

In zone-melting recrystallization of Si films on SiO_2, encapsulated with SiO_2/Si_3N_4, subboundaries form which correspond to small angular deviations $< 1°$. These have been entrained to form along parallel lines underneath a photolithographically-defined optical absorber pattern. Models for the generation and entrainment of subboundaries and grain boundaries are presented and supported by experimental results. Subboundary entrainment requires control of the temperature gradient, the modulation of the isothermal contours and the azimuthal crystallographic orientation.

Zone-melting recrystallization is a process in which a narrow molten zone produced in a thin film on a substrate is scanned across the sample (1-6), resulting in a film consisting of one or more large grains. Recent work has focused almost exclusively on Si over SiO_2 (4-6); whereas, earlier work dealt with Ge and InSb (2-3). The zone-melting recrystallization process is a simple solidification from the melt, and for this reason, the molten zone can be produced by any of several methods: laser, electron beam, arc lamp, hot wire, or (as in most of our work) graphite strip-heater (4-6). To confine the molten zone and prevent agglomeration or "balling up," an encapsulation layer is generally necessary, unless the zone is so narrow that agglomeration does not occur. Zone-melting recrystallization of Si on an SiO_2 substrate produces films composed of a few large grains, ~1 mm wide, extending the full length of the region scanned and having (100) texture (6). The <100> directions are generally within ~15° of the scan direction. Films of a single orientation have been produced by seeding from a single crystal (7-9), by zone-melting through planar constrictions (10, 11), and by so-called cross-seeding (5). In all cases, the films contain subboundaries which are arrays of dislocations or, equivalently, low-angle grain boundaries. (We use the term subboundary to refer to those low-angle boundaries which form during solidification from a single seed. We use the term grain boundary to refer to the region where crystals grown from two different seeds meet.) Subboundaries can be revealed by chemical etching. The crystallographic angular deviation across a subboundary is generally less than 1° (6, 12). The density of subboundaries can be substantially reduced by repeated melting and resolidification (13). This technique has been used to laser-recrystallize Si stripes, ~50 μm wide, essentially free of subboundaries (14). Subboundaries have also been eliminated by zone melting Si patterned into stripes (11).

Subboundaries have only a small effect on electron transport and do not inhibit the fabrication or operation of metal-oxide-silicon field-effect transistors that have minimum linewidths of several micrometers (15, 16). At present, it is not clear what effect subboundaries will have on other classes of devices. In this paper, we describe the entrainment of subboundaries and grain boundaries in strip-heater zone-melting recrystallization of Si using photolithographically-defined patterns that modulate the solidification front, and present models to explain the experimental results. Coligne *et al.* (17, 18) have used a patterned antireflection coating in conjunction with laser recrystallization to achieve grain boundary localization, although in this case, crystallographic texture was not controlled. The localization of subboundaries at well-defined positions gives one the option of building electronic devices between subboundaries in dislocation-free material. Moreover, the entrained subboundaries could perhaps play a beneficial role as gettering sites for certain mobile impurities and defects.

Method of Entrainment

Subboundaries arise when large facets form at the solid-liquid interface, as in the case of zone-melting recrystallization of Si with a graphite strip-heater. The subboundaries originate at the interior corners of the faceted front where two (111) planes meet (6), as shown in Fig. 1 and discussed more fully in the next section. Ordinary grain boundaries also locate at the interior corners. To entrain subboundaries and grain boundaries, one needs to control the positions of the

* Electrochemical Society Active Member.
[1] Also the Department of Electrical Engineering and Computer Science, Massachusetts Institute of Technology, Cambridge, Massachusetts 02139.
Key words: semiconductor, crystallography, solidification, crystallization.

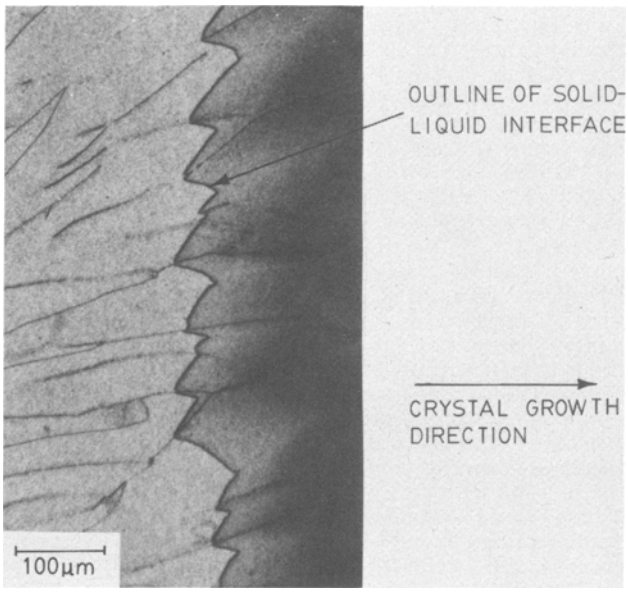

Fig. 1. Micrograph showing faceting of the solidification front in zone-melting recrystallization, and the formation of subboundaries at the interior corners. The means used to obtain the micrograph (6) is such that only the general morphology is revealed, not the instantaneous interface.

facet intersections during zone-melting recrystallization. One technique we have used for doing this is to spatially modulate the temperature at the solid-liquid interface. This can be done by forming a grating on top of the sample that locally enhances either the absorption or reflection of the radiation incident from above (19). Figure 2a illustrates schematically the use of a patterned optical absorber for subboundary entrainment. Figure 2b indicates entrainment of subboundaries underneath the absorber stripes. Because of the enhanced optical absorption, the Si is hotter under the middle of the absorber stripe than at any other lateral position, and hence, this is the last place to solidify. For this reason, the interior corners of the faceted solidification front, and hence, the subboundaries, align with the middle of the absorber, as depicted in Fig. 2b. As an optical absorber, we have used carbonized photoresist. Some results are shown in Fig. 3a. The Si film was 1 μm thick, the substrate was 1 μm of SiO_2 over a (100) Si wafer, the encapsulant was 2 μm SiO_2 and 30 nm Si_3N_4, and the entrainment pattern was a grating of carbonized photoresist (AZ1350 J, Shipley Company, Newton, Massachusetts, initially ~7 μm thick) of 100 μm period and 50 μm linewidth. The zone melting was carried out at a scanning speed of 0.5-1 mm/sec, as described in detail in Ref. (5, 6). The Si between entrained subboundaries is free of dislocations, as determined by chemical etching, and no carbon contamination was detected by Auger analysis, implying that any contamination must be $<10^{19}$ atom/cm^3. Figure 3b shows the typical pattern of subboundaries from an area of an identical sample that did not have an entrainment pattern.

Figure 4 illustrates the use of a grating of thin Si stripes imbedded in an encapsulation layer to achieve entrainment. The thin Si stripes reflect incident radiation at the high temperature used in zone melting, and, as a result, subboundaries entrain between the Si stripes.

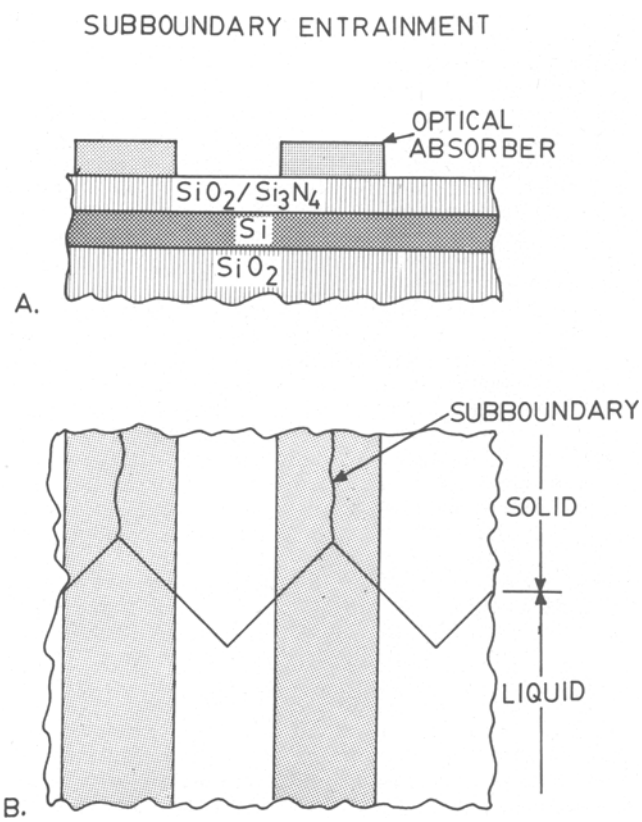

Fig. 2. (a) Schematic illustration of the use of a grating of optical absorber stripes on top of an encapsulation layer to modulate the temperature profile and entrain subboundaries. (b) Illustration of the entrainment of subboundaries under the middle of the optical absorber stripes.

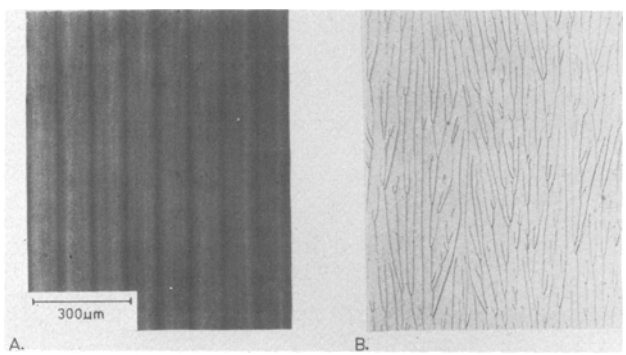

Fig. 3. (a) Entrainment of subboundaries in a 1 μm thick Si film using a 100 μm period, 50 μm linewidth, grating of carbonized photoresist. (b) Typical pattern of subboundaries in an identical sample recrystallized without an entrainment pattern.

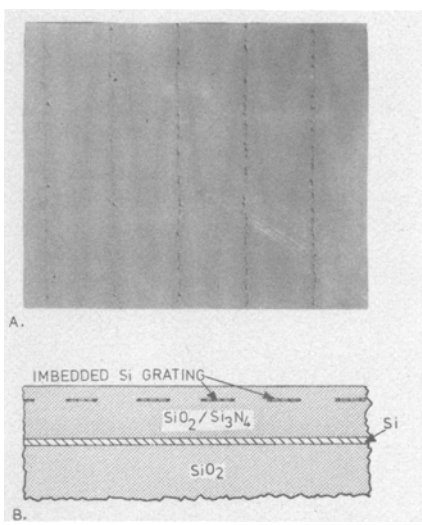

Fig. 4. (a) Entrainment obtained with a grating of Si stripes imbedded in an encapsulation layer. The stripes are reflecting and, as a result, entrainment occurs in between stripes. (b) Schematic illustration of the imbedded Si reflector stripes.

Mechanism of Subboundary Entrainment

The results presented in the previous section demonstrate the feasibility of entraining subboundaries. In this section, we present a model to explain the characteristic morphology of subboundaries, and support this with experimental evidence. Following that, we develop a model for subboundary entrainment and present experimental results which indicate that the modulation depth, temperature gradient, and azimuthal crystallographic orientation must be controlled within narrow ranges in order to entrain subboundaries. Such control has been difficult to achieve with current strip-heater techniques, and, as a result, we have not been able to entrain subboundaries over an entire sample, or to get consistency from run to run. Despite this lack of consistency, we believe our results point the way to further improvements in subboundary entrainment.

Figure 1 shows that the solid-liquid interface of Si is faceted in zone-melting recrystallization. (To obtain this micrograph the molten zone was rapidly quenched with a jet of He gas during scanning (6). This method reveals the general morphology of the solid-liquid interface but does not provide an instantaneous demarcation as given, for example, in Fig. 6 below.) A faceted interface is consistent with Jackson's criterion (20, 21) and also indicates that growth occurs by the addition of atoms at ledges or steps which sweep rapidly across the facets. Subboundaries originate at the interior corners of the faceted solid-liquid interface. Figures 1 and 3b show the typical morphology of subboundaries. The initiation of new subboundaries between two approximately parallel subboundaries and the coalescence of two subboundaries to form a "Y" or "wishbone" pattern are characteristic morphological features. Figure 5 depicts a simplified model of the solid-liquid interface at three consecutive times, and indicates how new subboundaries originate and form the characteristic "wishbone" patterns. The Si film is assumed to have a (100) texture with <100> direction parallel to the direction of zone motion. The facets at the liquid-solid interface are (111) planes,

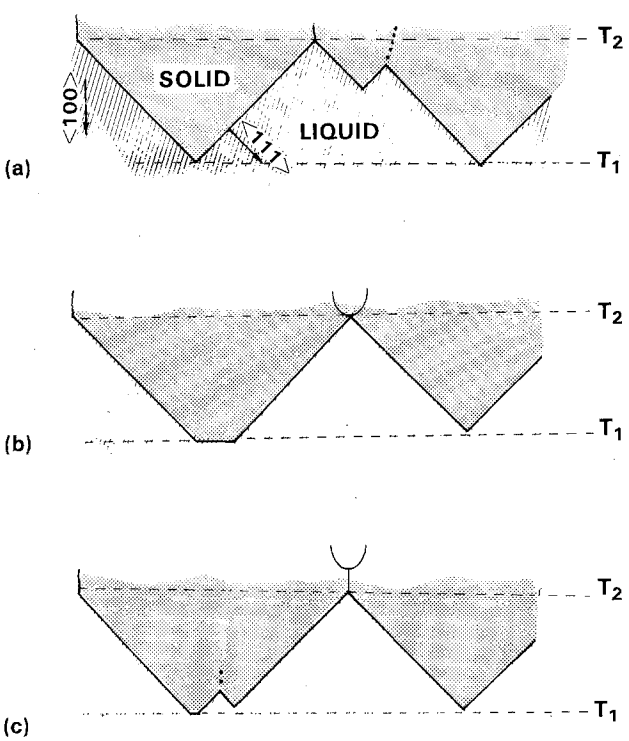

Fig. 5. Simplified model of the solid-liquid interface, shown as a top view, at three consecutive times. The isothermal contours, T_1 and T_2, are defined in the text. Subboundaries are shown originating at interior corners. The characteristic Y or "wishbone" pattern is due to the coalescence of two interior corners.

and, thus, their intersections with a plane parallel to the substrate form 90° angles. The distance a chevron-shaped pair of facets extends into the liquid silicon, which determines the distance between the subboundaries originating at the interior corners, is limited by two temperatures, T_1 and T_2, shown as dotted isothermal contours in Fig. 5. T_2 is the temperature at which the generation of new ledges occurs at such a rate that the forward advance of the (111) facets just matches the imposed zone-scanning velocity. At temperatures close to T_2, the speed with which ledges sweep across a (111) facet is much greater than the rate of forward advance of the solidification front; hence, the rate of forward advance is determined by the rate of generation of new ledges at T_2. The velocity of ledge motion decreases as a ledge encounters higher and higher temperatures. Eventually, when T_1 is reached, the forward velocity of the ledge just matches the zone-scanning velocity. T_1 is probably very close to the melting temperature of Si, T_m. Liquid silicon can, of course, be undercooled more than $T_m - T_2$. At higher undercoolings, however, ledge nucleation at reentrant corners, and at the intersection of the crystalline silicon with the cap and substrate, will be even more copious than at T_2, and for this reason, the solidification front should not fall behind T_2. One might propose other mechanisms (22, 23) but regardless of which mechanism operates, we believe Fig. 5 depicts a reasonable working model of the behavior of the solid-liquid interface. If impurities are present in the molten Si, they would tend to segregate at interior corners, thus, lowering the local solidification temperature, causing cul-de-sacs to form that trail behind the T_2 contour.

Subboundaries tend to be parallel to the direction of zone motion but small perturbations can cause them to move laterally. When the distance between adjacent subboundaries becomes so large that the chevron formed by a pair of facets would extend beyond T_1, the front of the chevron becomes flattened, as indicated in Fig. 5b. This flattened face is not stable and soon dimples and develops into an interior corner which becomes a source of dislocations, as depicted in Fig. 5c. This interior corner will not advance at the imposed scanning velocity but instead will fall back until it contacts the contour T_1. Figures 5a-c also illustrate the coalescence of two subboundaries to create the characteristic wishbone pattern. Note that the apex of a wishbone is parabolic rather than angular. This indicates that some mechanism causes interior corners to pull together when they come within a few micrometers of one another.

Figure 6 provides experimental evidence for the model presented in Fig. 5, showing both formation of new subboundaries by the flattening-dimpling mechanism and the coalescence of subboundaries to form a wishbone. The micrograph was obtained from an Si film which was etched after zone-melting recrystallization to delineate subboundaries, which appear as dark vertical lines, and dopant variations in the film, which appear as zig-zag horizontal lines. The dopant variations were obtained by pulsing the upper heater strip at 120 Hz to demark the instantaneous solid-liquid interface. (This technique was previously used by Holmes *et al.* (24) for the case of conventional crystal growth from the melt.) Approximately every twelfth demarcation line in Fig. 6 is traced in ink to clarify the time evolution of the solidification front. The formation of cul-de-sacs at the interior corners can also be inferred from the slight curvature of certain demarcation lines as they near the interior corners. The protrusions frequently observed along subboundaries (6, 12, 25) are also consistent with cul-de-sac formation and delayed solidification. Leamy *et al.* have presented evidence for cellular growth in strip-heater zone-melting recrystallization at high impurity content (26, 27). Our observations of the zone-melting recrystallization of Si films heavily doped with As are

Fig. 6. Micrograph of an Si film recrystallized by zone-melting showing experimental evidence in support of the model presented in Fig. 5. The instantaneous solid-liquid interface was demarked by pulsing the upper strip-heater at 120 Hz. Approximately every twelfth demarcation line is traced in ink to clarify the time evolution of the solidification front. Seam direction is from top to bottom.

consistent with this (6). However, Fig. 10 of Ref. (6) showed that increased speed of zone motion led to an increase in subboundary spacing in undoped Si, which argues against a cellular-growth mechanism of subboundary formation. Faceting similar to that shown in Fig. 6 has been observed in bulk crystal growth (28).

When an absorbing or reflecting grating pattern is located above a film being recrystallized by the zone-melting technique, the temperature profile is modulated. Figures 7a and b depict two different depths of sinusoidal modulation that have the same temperature gradient (*i.e.*, the same distance between T_2 and T_1 contours). In Fig. 7a, the depth of modulation is small, subboundaries form between entrained subboundaries, and move laterally. We have frequently observed patterns of subboundaries that can be explained by the model of Fig. 7a. In Fig. 7b, the depth of modulation is large enough to prevent the formation of subboundaries between those that are entrained. The portion of the solid-liquid interface located along the isothermal contour T_2 does not give rise to dislocations or subboundaries, and, hence, we assume it is microscopically faceted and able to follow the curvature of the contour, as depicted in Fig. 7b. According to this model, entrainment without the generation of additional, non-entrained subboundaries requires a modulation of the T_2 contour given by

$$Y \geqq (0.22D) \sin (2\pi X/D)$$

where the distance, Y, is in the direction of zone motion, D is the period of the entrainment pattern, and X is a distance measured perpendicular to the direction of zone motion. Unfortunately, we have not been able to directly monitor the temperature contours or the entrained solidification fronts and, hence, could not confirm our models experimentally. However, we did

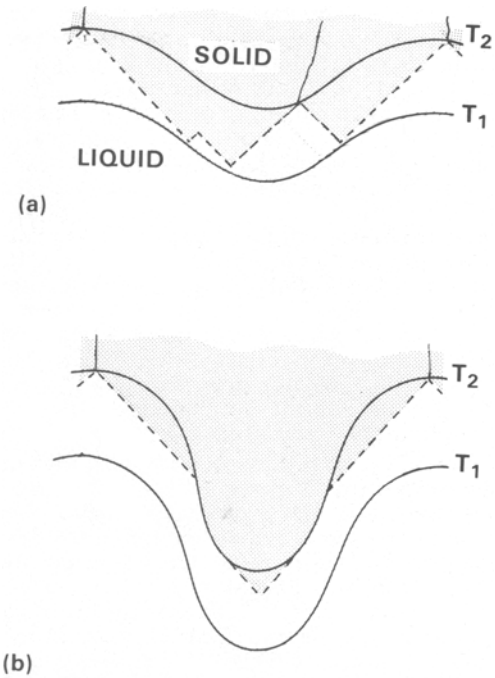

Fig. 7. Schematic illustration of a model for the solid-liquid interface when the isothermal contours are sinusoidally modulated. (a) Depth of modulation is insufficient to achieve full entrainment. (b) Depth of modulation is sufficient to induce entrainment.

observe that entrainment was favored by increased temperature modulation.

Control of the temperature gradient is important in subboundary entrainment. Before discussing this, it is helpful first to clarify the relationship between temperature gradient and subboundary spacing. As discussed above and in Ref. (6), the average separation between subboundaries in zone-melting recrystallization depends upon the distance a chevron-shaped pair of facets extends into the molten Si, which in turn depends upon the temperature gradient, specifically the distance between the T_1 and T_2 contours. This was confirmed experimentally, as shown in Fig. 8. In Fig. 8a, the upper heater was a single strip of graphite, whereas, in Fig. 8b, two strips were used to reduce the temperature gradient. As shown in the micrographs, the average subboundary spacing increases as the gradient is decreased. (A similar result was reported in Ref. (6), Fig. 10, where decreased tempera-

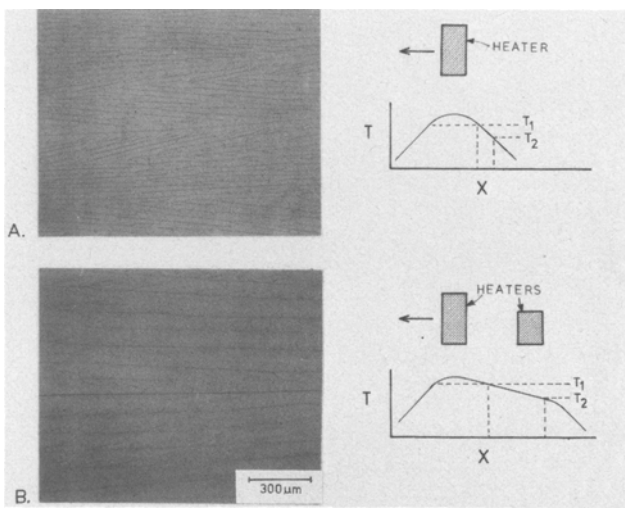

Fig. 8. Dependence of subboundary spacing on temperature gradient. (a) A single strip-heater yields a normal subboundary spacing (6). (b) A shallower temperature gradient, produced by a pair of strip-heaters, yields an increased subboundary spacing.

ture gradient was achieved by increasing the speed of zone motion.) We were able to get entrainment only when the period of the entrainment pattern, D, was at least a factor of 2 larger than the average separation between subboundaries, reflecting the need for a steep thermal gradient to achieve entrainment.

Figure 9 illustrates the importance of azimuthal crystallographic orientation in entrainment. The grid of etch pits (29) shows that two crystal grains are present and that the grain boundary is entrained. On the lower side of the grain boundary, the <100> direction is parallel to the lines of the entrainment pattern. On the upper side, the <100> direction is at an angle of ~40° to the entrainment lines. As a result of this azimuthal misorientation, the pattern of subboundaries has an asymmetric "feathered" appearance due to subboundaries that originate in between the entrained boundaries and run roughly parallel to the $<0\bar{1}0>$ direction until they coalesce with the entrained boundaries. Figure 10 presents a simplified model, for the case where the <100> direction is rotated approximately 25° from the growth direction, illustrating how this asymmetric pattern of subboundaries probably occurs. At time, t_1, a single interior corner is shown, located on the T_2 contour. This interior corner and the region where the chevron facet is tangent to the T_2 contour are sources of ledges which sweep across the facets of the chevron, causing it to grow. When the tip of the chevron encounters the T_1 contour a new interior corner is formed, as depicted at t_2. (This dimpling mechanism was discussed in connection with Fig. 5.) The newly formed interior corner falls back until it encounters the T_2 contour, as depicted at t_3. Since an interior corner cannot trail behind the T_2 contour, the forward motion of the contour causes the interior corner to move to the left, as shown at t_4. As an interior corner approaches the peak of the contour the leftward movement ceases and coalescence with

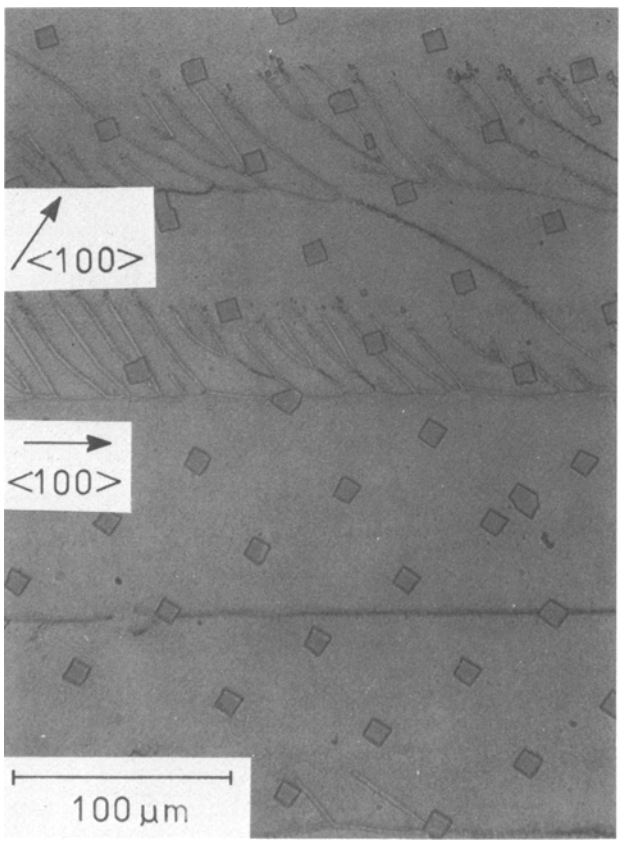

Fig. 9. Optical micrograph showing the dependence of entrainment on azimuthal crystallographic orientation. The diagonals of the etch pits are <100> directions.

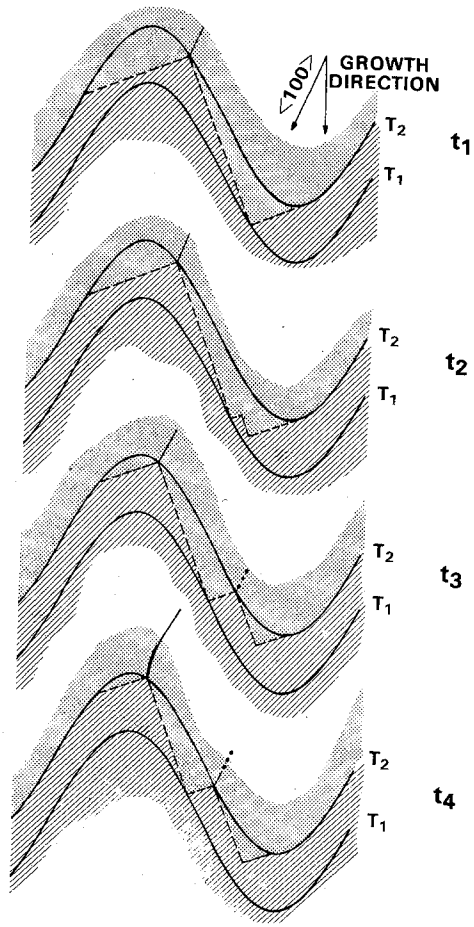

Fig. 10. Schematic illustration of a model for the solid-liquid interface at four consecutive times, t_1, t_2, t_3, and t_4, when the <100> crystallographic direction is at an angle relative to the direction of zone motion. The direction of zone motion is parallel to the entrainment pattern axis.

an interior corner entrained at the peak should occur (not shown in Fig. 10). A subboundary traces the path of the interior corner from which it originates. Thus, subboundaries are initially parallel to the <100> direction but as they approach the peak of the T_2 contour they follow the growth direction and coalesce. This model is certainly a simplification but predicts a subboundary pattern reasonably close to that observed in Fig. 9.

Conclusions

We have described the entrainment, by means of photolithographically defined patterns, of subboundaries and grain boundaries in zone-melting recrystallization of Si over SiO_2. A model for the generation and characteristic morphology of subboundaries was presented, and we showed that entrainment requires a high degree of control over the temperature gradient, the modulation of the isothermal contours, and the azimuthal crystallographic orientation. Recrystallized samples of Si-on-SiO_2 in which the subboundaries are entrained may be ideal for integrated electronic circuits because critical regions of devices could be arranged to avoid the subboundaries, and subboundaries could serve as getter sites.

Acknowledgments

The authors are grateful to C. L. Doherty, K. E. Krohn, J. M. Lawless, and G. H. Foley for technical assistance, and M. Finn for Auger analysis. This work was sponsored by the Defense Advanced Research Projects Agency, the Department of the Air Force, and the Department of Energy.

Manuscript submitted Sept. 15, 1982; revised manuscript received Jan. 3, 1983.

Any discussion of this paper will appear in a Discussion Section to be published in the December 1983 JOURNAL. All discussions for the December 1983 Discussion Section should be submitted by Aug. 1, 1983.

Publication costs of this article were assisted by Massachusetts Institute of Technology.

REFERENCES

1. E. Leitz, British Pat. 691,335 (1953).
2. J. Maserjian, *Solid-State Electron.*, **6**, 477 (1963).
3. A. R. Billings, *J. Vac. Sci. Technol.*, **6**, 757 (1969).
4. E. W. Maby, M. W. Geis, Y. L. LeCoz, D. J. Silversmith, R. W. Mountain, and D. A. Antoniadis, *Electron. Device Lett.*, **edl-2**, 241 (1981).
5. M. W. Geis, H. I. Smith, B-Y. Tsaur, J. C. C. Fan, E. W. Maby, and D. A. Antoniadis, *Appl. Phys. Lett.*, **40**, 158 (1982).
6. M. W. Geis, H. I. Smith, B-Y. Tsaur, J. C. C. Fan, D. J. Silversmith, and R. W. Mountain, *This Journal*, **129**, 2813 (1982); M. W. Geis, H. I. Smith, B-Y. Tsaur, J. C. C. Fan, D. J. Silversmith, R. W. Mountain, and R. L. Chapman, in "Proceedings of the 1982 Materials Research Society Conference," Boston, MA, November 1982.
7. J. C. C. Fan, M. W. Geis, and B-Y. Tsaur, *Appl. Phys. Lett.*, **38**, 365 (1981).
8. B-Y. Tsaur, M. W. Geis, J. C. C. Fan, D. J. Silversmith, and R. W. Mountain, *ibid.*, **39**, 909 (1981).
9. R. F. Pinizzotto, H. W. Lam, and B. L. Vaandrager, *ibid.*, **40**, 388 (1982).
10. H. I. Smith, H. A. Atwater, and M. W. Geis, Paper 159 presented at The Electrochemical Society Meeting, Montreal, Que., Canada., May 9-14, 1982.
11. H. A. Atwater, H. I. Smith, and M. W. Geis, *Appl. Phys. Lett.*, **41**, 747 (1982).
12. H. W. Lam, R. F. Pinizzotto, D. S. D. Malhi, and B. L. Vaandrager, *ibid.*, **41**, 1083 (1982).
13. K. A. Jackson and C. E. Miller, *J. Cryst. Growth*, **42**, 364 (1977).
14. G. K. Celler, L. E. Trimble, K. K. Ny, H. Baumgart, and H. J. Leamy, Paper 151 presented at the Electrochemical Society Meeting, Montreal, Que., Canada, May 9-14, 1982.
15. E. W. Maby and D. A. Antoniadis, *Appl. Phys. Lett.*, **40**, 158 (1982).
16. B-Y. Tsaur, J. C. C. Fan, M. W. Geis, D. J. Silversmith, and R. W. Mountain, *IEEE Electron Device Lett.*, **edl-3**, 79 (1982).
17. J. P. Colinge, G. Auvert, and J. M. Temerson, Paper 147 presented at The Electrochemical Society Meeting, Montreal, Que., Canada, May 9-14. 1982.
18. J. P. Colinge, E. Demoulin, D. Bensahel, and G. Auvert, *Appl. Phys. Lett.*, **41**, 346 (1982).
19. M. W. Geis, H. I. Smith, B-Y. Tsaur, J. C. C. Fan, D. J. Silversmith, and R. W. Mountain, Electronic Materials Conference, Fort Collins, CO, June 1982.
20. D. P. Woodruff, "The Solid-Liquid Interface," Chap. 3, Cambridge University Press, New York (1973).
21. K. A. Jackson, in "Nucleation and Atomic Kinetics," North Holland, New York (1979).
22. D. E. Ovsienko and G. A. Alfinstev, in "Crystals Growth, Properties, and Applications," pp. 119-170, Springer-Verlag, Berlin, Heidelberg, New York (1980).
23. J. W. Cahn, *Acta Metall.*, **8**, 554 (1960).
24. D. E. Holmes and H. C. Gatos, *J. Appl. Phys.*, **52**, 2971 (1981).
25. J. C. C. Fan, B-Y. Tsaur, R. L. Chapman, and M. W. Geis, *ibid.*, **41**, 186 (1982).
26. H. J. Leamy, C. C. Chang, H. Baumgart, R. A. Lemons, and J. Chang, *Mater. Lett.*, **1**, 33 (1982).
27. R. A. Lemons, M. A. Bosch, J. Cheng, and H. J. Leamy, Electronic Materials Conference, Fort Collins, CO, June 1982.
28. W. Bardsley, J. S. Boulton, and D. T. J. Hurle, *Solid-State Electron.*, **3**, 395 (1962).
29. K. A. Bezjian, H. I. Smith, J. M. Carter, and M. W. Geis, *This Journal*, **129**, 1848 (1982).

Mass Spectrographic Analysis and SEM Investigation of α-HgI_2 Crystals Grown by Static Sublimation

T. Kobayashi,[1] J. T. Muheim, P. Waegli, and E. Kaldis

Laboratorium für Festkörperphysik, ETHZ, 8093 Zürich, Switzerland

ABSTRACT

In this paper, the applicability of spark-source mass spectrographic analysis and SEM investigations for α-HgI_2 is demonstrated. The influence of the chemical history of the material on the spectrum of the impurities has been investigated by comparing materials synthesized in three different ways. Static sublimation was used to grow single crystals, which had an appreciable average linear growth rate (10^{-6} cm/sec) and relatively low etch pit density (10^3/cm^2 or less). Synthesis from "suprapur" elements after additional purification of iodine gave the most pure crystals, which still contained 1700 ppm at. of impurities. The spark source mass spectrographic analysis on α-HgI_2 reveals abundant distributions which are conspicuously characteristic of the crystal properties (valence, structure, composition, etc.) for elemental impurities, and crystal structure characteristic for the hydrocarbon fragments. Overall abundances for sublimated α-HgI_2 vary according to the material source. Morphological investigation of uncoated crystal surfaces (as grown, etched, or cleaved) was possible by low temperature SEM investigation. They showed that most etch pits are flat bottomed at up to 10,000× magnification. Emergence points of dislocations are not visible; dislocations appear only in the form of a few pyramidal etch pits.

Red tetragonal mercuric iodide (α-HgI_2) has been receiving much attention as a material for room temperature operable semiconductor detectors for low energy x- and γ-rays (1-3). This is due to its unique physical properties. Its wide bandgap of 2.1 eV, and the large atomic numbers of the components (80 for Hg and 53 for I) result in low dark current at room temperature and high photoionization efficiency (1, 2). A medical application was exemplified by a small HgI_2 detector mounted inside an injection needle (4). Application to computer tomography is highly desirable if small size HgI_2 detectors could replace the currently used large scintillation detectors. In this way, the local resolution of the tomograms would be improved.

In the last six years, considerable progress has been made in crystal growth of α-HgI_2 and detector fabrication. However, the detector performance of HgI_2 tends to suffer from insufficient collection of the electrons and holes, produced by the interaction of an incident photon with the crystal. This is due to rather

[1] Permanent address: The Graduate School at Nagatsuta, Tokyo Institute of Technology, Midori-Ku Jokohama 227, Japan.

Key words: α-HgI_2, single crystals by static sublimation, impurities in, mass spectrographic analysis of, SEM investigation on cold stage, spark source mass spectrographic analysis of HgI_2, sublimation, static, of αHgI_2, vapor growth rate of α-HgI_2 single crystals.